E13-2025-50

Yu. S. Tsyganov [1,*], D. A. Ibadullayev [1,2], A. N. Polyakov [1],
M. V. Shumeiko [1], A. A. Voinov [1]

DETECTION SYSTEM OF **DGFRS-2** SETUP: SIMULATION OF HEAVY RECOIL SPECTRA AND RADIATION LIMITS

Submitted to Eurasian Journal of Physics and Functional Materials

[1] Joint Institute for Nuclear Research, Dubna, Russia
[2] Institute of Nuclear Physics, Almaty, Kazakhstan
[*] E-mail: tyra@jinr.ru

Цыганов Ю. С. и др. E13-2025-50

Детектирующая система установки DGFRS-2: моделирование спектров ядер отдачи и радиационные лимиты

Детектирующая система установки DGFRS-2 применялась в длительных экспериментах с пучками ионов ^{40}Ar, ^{48}Ca, ^{50}Ti и ^{54}Cr, ускоряемыми сверхинтенсивным циклотроном DC-280 в Лаборатории ядерных реакций им. Г. Н. Флерова ОИЯИ. Зарегистрированные спектры энергии сверхтяжелых ядер сравнивались с расчетными спектрами, и было достигнуто удовлетворительное согласие. Кроме того, исследовались радиационные эффекты, наблюдавшиеся при длительном облучении. К ним относятся рост тока утечки в фокальном DSSD-детекторе, а также ограничения на использование кремниевых детекторов и применение моделирования спектров ER в длительных экспериментах. Приведен репрезентативный пример, иллюстрирующий увеличение тока утечки DSSD-детектора в ходе эксперимента. Предпринята попытка предсказать срок службы DSSD-детектора в экспериментах по ядерным реакциям, индуцированным тяжелыми ионами, на установке DGFRS-2, основанная на простом масштабировании эффектов радиационных повреждений с использованием концепции потерь энергии на неионизирующие процессы (NIEL).

Работа выполнена в Лаборатории ядерных реакций им. Г. Н. Флерова ОИЯИ.

Препринт Объединенного института ядерных исследований. Дубна, 2025

Tsyganov Yu. S. et al. E13-2025-50

Detection System of DGFRS-2 Setup: Simulation of Heavy Recoil Spectra and Radiation Limits

The detection system of the DGFRS-2 setup was employed in long-term experiments using ion beams of ^{40}Ar, ^{48}Ca, ^{50}Ti, and ^{54}Cr generated by the DC-280 ultraintense cyclotron at the Flerov Laboratory of Nuclear Reactions (JINR). The registered energy spectra of recoiled superheavy nuclei were compared to calculated spectra and satisfactory agreement was achieved. Additionally, radiation effects observed during prolonged irradiation were investigated. These effects included the growth of leakage current in the DSSD focal detector as well as limitations on the use of silicon detectors and the application of ER spectra modeling in long-term heavy-ion beam experiments. A representative example illustrating the increase in leakage current of a DSSD detector during the experiment is presented. An attempt to predict the lifetime of the DSSD detector in heavy-ion-induced nuclear reaction experiments at the DGFRS-2 setup is proposed, based on simple scaling of radiation damage effects using the non-ionizing energy loss (NIEL) concept.

The investigation has been performed at the Flerov Laboratory of Nuclear Reactions, JINR.

Preprint of the Joint Institute for Nuclear Research. Dubna, 2025

INTRODUCTION

The most profound insights into nuclear structure are often obtained through the study of nuclei under extreme conditions. Superheavy nuclei (SHN) serve as a prime example, as their large proton numbers lead to intense Coulomb repulsion, making them inherently unstable against spontaneous fission. However, quantum shell effects provide additional stability, enabling the existence of these nuclei. Several theoretical models predict an "island of stability" [1] — a region around element 114 (flerovium), where nuclei are expected to exhibit significantly increased half-lives relative to those outside this region.

Since 1998, the Flerov Laboratory of Nuclear Reactions (FLNR) at JINR has conducted a systematic program of superheavy element synthesis using the Dubna Gas-Filled Recoil Separator (DGFRS) [2, 3]. These experiments employed complete fusion reactions between ^{48}Ca ion beams and actinide targets. Between 1998 and 2002, new elements from flerovium (114) to oganesson (118) were discovered at FLNR in reactions of ^{48}Ca with actinide targets of ^{242,244}Pu,^{243}Am,^{245,248}Cm, ^{249}Bk, ^{249}Cf [4–8]. Several of these findings were later independently confirmed at other international facilities, including SHIP (GSI, Germany), BGS (Berkeley, USA), TASCA (GSI, Germany), GARIS (RIKEN, Japan), and SHANS-1, SHANS-2 (IMP, China) [9–15].

The synthesis of these elements was made possible by the use of advanced gas-filled recoil separators and highly sensitive detection systems capable of identifying rare α-decay chains and spontaneous fission events amidst substantial background. These systems were crucial in reactions of the type $^{48}\mathrm{Ca} + \text{actinide target} \rightarrow \mathrm{SHN} + xn$ carried out at the U-400 cyclotron. The observed production cross sections range from 0.1 to 10 pb. However, future experiments on the synthesis of elements with $Z > 118$ involving heavier projectiles, such as ^{50}Ti and ^{54}Cr, are expected to result in significantly reduced cross sections, thereby imposing more stringent requirements on the performance of both separators and detection systems.

For further experiments, the new Superheavy Element Factory and the DGFRS-2 separator were put into operation in 2020. The separator uses intense (2–7 $p\mu$A) heavy-ion beams from the DC-280 cyclotron [16]. During this period, the following experiments were carried out [17–20].

Initially, the accelerated ions strike the target. As a result of a complete fusion reaction — occurring with a very low probability — a compound nucleus is formed in an excited state. In order to transit to its ground state without losing protons, the nucleus must emit several neutrons and gamma rays. The recoiled nuclei, ejected from the target due to the momentum imparted by the bombarding particles (e.g., ^{48}Ca), enter the

DGFRS-2 separator. There, they are first vertically focused in-flight by the Q_1 quadrupole lens to pass through the gap of the D_1 dipole magnet, which separates heavy nuclei from background particles. Afterward, the recoils are additionally focused by Q_2 (horizontally) and Q_3 (vertically), then pass through the D_2 magnet, which removes lighter particles (such as protons and α particles), before reaching the detector chamber. The DGFRS-2 separator is filled with hydrogen gas at a pressure of approximately 0.7 Torr. The detector chamber is separated from the separator volume by a 0.8-μm-thick Mylar window and is filled with pentane gas at 1.2 Torr. To detect rare events of superheavy nuclei decay, the detection module shown in Fig. 1 [21–23] was used. Regular leakage current measurements were conducted to assess the detector's radiation damage.

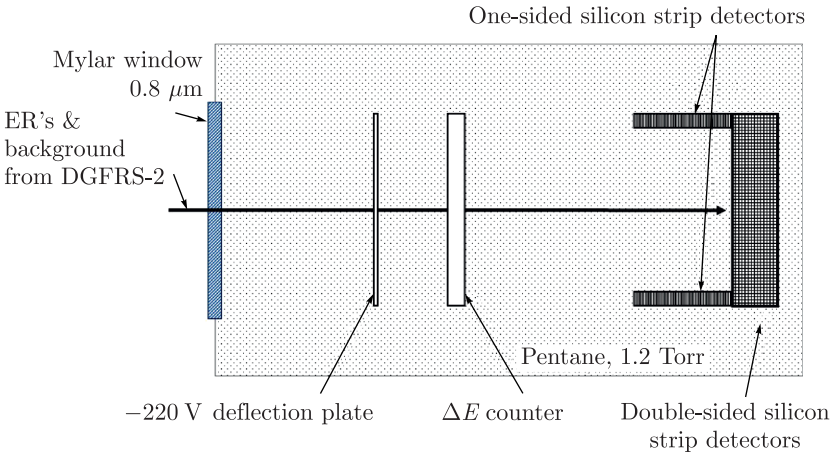

Fig. 1. Schematics of the detection module of the DGFRS-2 setup (not to scale)

The system is based on a DSSD detector for recording the decays of superheavy nuclei and a low-fission gas module for detecting recoiled nuclei and other charged particles moving outward from the cyclotron. Note that DSSD detectors are widely used in science and not only in the facilities like gas-filled separators [13, 24–29].

1. ENERGY SPECTRA OF RECOILED SUPERHEAVY NUCLEI DETECTED WITH THE SILICON RADIATION DETECTOR

In the experiments on the synthesis of superheavy elements (SHE), a specialized registration method known as "active correlation technique" is employed. It enables registration of α decays from daughter products in a virtually background-free mode by switching off the cyclotron beam for the decay time after detecting the ER–α correlation link in real time.

The idea behind the "active correlations" method for real-time operation is to create two discrete (matrix-based) virtual objects ("detectors") in the memory of the detection system's computer. Specifically, these are the recoil (ER) and α-particle matrixes, each with a discretization of $X * Y$. Here, X and Y represent the number of horizontal and vertical strips, respectively. Naturally, before this, the experimenter defines the ER and alpha-decay objects as part of the preliminary conditions file.

The matrix elements contain the current time obtained from the hardware (or the Windows system clock). When a signal of α type is received, it is compared with the corresponding element of the ER matrix. If the time difference $t_{ij}(\alpha) - t_{ij}(\mathrm{ER}) < \varepsilon$, the irradiation process is paused for a duration of Δt. If an alpha decay is registered during the beam-off pause, and it falls within a predefined energy range and the same position, the beam-off phase is extended. Edge effects between neighboring strips are naturally taken into account [21, 30]. An alternative version of the trigger is also possible, using ER–α–α instead of the standard ER–α [31]. Over the past two years, a more advanced version of this method has been tested, replacing the standard algorithm with a flexible one [22, 32, 33]. In essence, the experimenter sets an acceptable level of irradiation time loss, and the system automatically selects the correlation time interval in an adaptive mode. It is believed that this algorithm may be most efficient at titanium beam currents around 10 $p\mu$A or slightly lower. Simplified versions are also possible, such as stopping solely by an alpha-decay signal (if the energy of the studied nuclide is known) or working with correlated signals while ignoring ΔE signals [33]. In details this method is described in [21, 30–34]. As a visual example, Fig. 2 shows the decay chain of flerovium from the experiment $^{242}\mathrm{Pu} + ^{48}\mathrm{Ca} \rightarrow {}^{287}\mathrm{Fl} + 3n$. After the detection system registered an ER–α correlation in real time, the beam was switched off (with a dead time of approximately 100 μs), and the

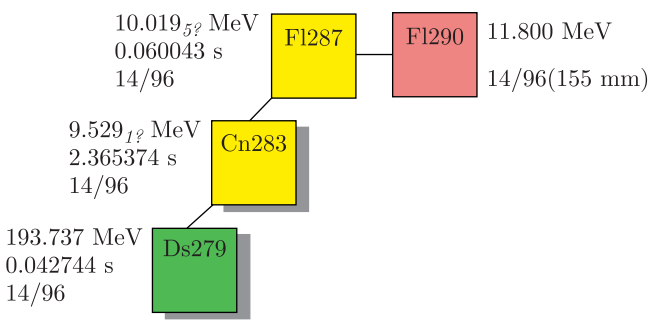

Fig. 2 (color online). Example of a decay chain of the ^{287}Fl nucleus. Shadows denote beam-off time interval after detecting ER–α sequence in a real time mode. The recoil nucleus is shown in pink, while the nuclei undergoing alpha decay and spontaneous fission are shown in yellow and green, respectively. The energy, coordinates, and decay time are also indicated

subsequent decays (indicated by the shaded area) occurred under virtually background-free conditions.

Consequently, understanding the shape of a recoiled heavy nucleus spectrum is relevant for both ongoing experiments and planned efforts to synthesize

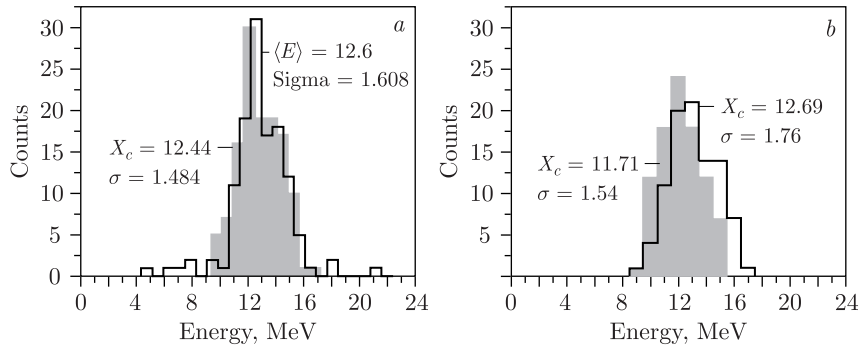

Fig. 3. *a*) Measured (black) and calculated (grey) spectra of Mc ER's. Reaction $^{243}\mathrm{Am} + ^{48}\mathrm{Ca} \rightarrow \mathrm{Mc}^*$. *b*) Measured (black) and calculated (grey) spectra of Fl ER's. Reaction $^{242}\mathrm{Pu} + ^{48}\mathrm{Ca} \rightarrow \mathrm{Fl}^*$

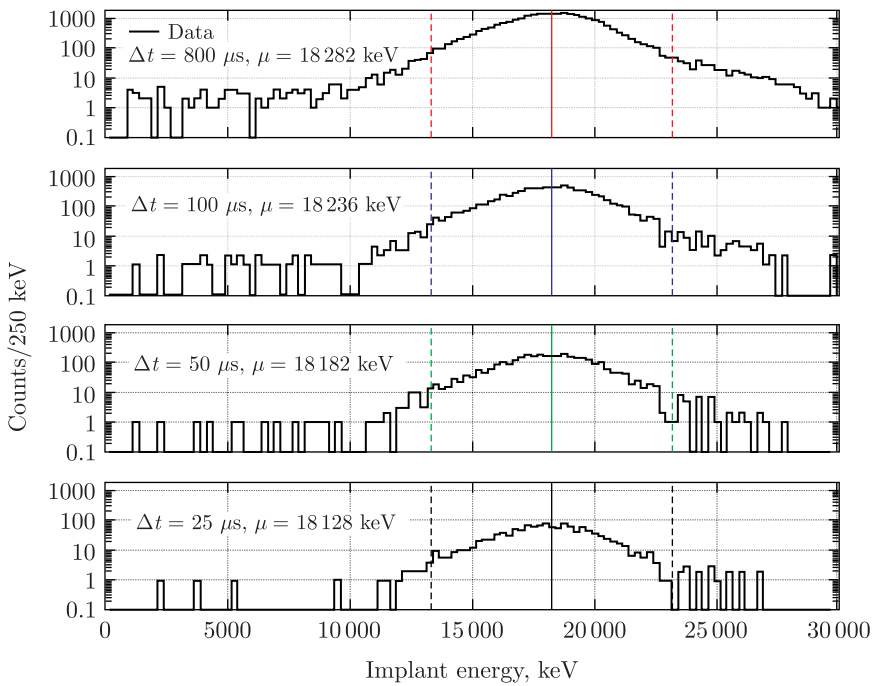

Fig. 4. Spectra of ^{217}Th ER for different correlation time intervals (centroids μ and interval values Δt are shown, dashed lines indicate +/− 3 sigma interval)

elements with $Z = 119$ and $Z = 120$ in the foreseeable future, particularly when using heavy-ion beams of ultrahigh intensity, up to approximately $\sim 5{-}10\ p\mu$A.

Figure 3 shows the spectra of the registered energy of implanted into silicon detector nuclei for the reactions $^{243}\mathrm{Am} + ^{48}\mathrm{Ca} \to \mathrm{Mc}^*$ and $^{242}\mathrm{Pu} + ^{48}\mathrm{Ca} \to \mathrm{Fl}^*$.

On the other hand, it should be noted that there are isolated events outside the $\pm 3\sigma$ standard deviation region. Below, in Fig. 4, the recoiled nuclei spectra from the calibration reaction $^{\mathrm{nat}}\mathrm{Yb} + ^{48}\mathrm{Ca} \to {}^{217}\mathrm{Th} + 3n$ are shown.

The presence of a right-hand tail in the spectrum is evident, whereas the left side is absent. The nature of these small deviations from the model spectrum may become one of the objectives of our future investigations. However, as a reasonable hypothesis, we can point to two possible processes responsible for the presence of the right-side tail of the distribution:

— channeling effect of heavy ions in silicon [35];

— strong asymmetry of non-ionizing energy loss (NIEL) fluctuations in silicon.

Table 1 below shows the events that fall outside the $\pm 3\sigma$ range of the main distribution. It should be noted that quantitatively these account for no more than approximately 2.8% of the total number of events.

Table 1. **Event distribution outside +/− 3 sigma**

^{217}Th dt(ER–α), μs Reaction $^{\mathrm{nat}}$Yb + ^{48}Ca	Mean value, keV	Standard deviation	Left/right outside +/− 3 sigma, % (with respect to total event number)
25	18 128	1656	1.18/1.34
50	18 182	1677	1.51/1.23
100	18 236	1639	1.55/1.36
800	18 282	1625	1.49/1.55

1.1. On the Registered Energy Spectra of ^{254}No Nucleus. When preparing this manuscript, experiment $^{241}\mathrm{Am} + ^{48}\mathrm{Ca} \to \mathrm{Mc}^*$ has been successfully finished [13–15] at the Institute of Modern Physics (Lanzhou, China). During that experiment, complete fusion nuclear reaction $^{208}\mathrm{Pb} + ^{48}\mathrm{Ca} \to {}^{254}\mathrm{No} + 2n$ was used for the sake of calibration and to test a whole electronics readiness. Below, in Fig. 5, *a*, spectra of ^{254}No ER's implanted into DSSD detector for different correlated time intervals are shown. It can be easily seen that for different time intervals the same shapes of those spectra are observed. In Fig. 5, *b*, simulated evaporation residues (ER) spectrum for nobelium (No) is presented.

The difference in the centroid position of about 0.9 MeV is measured and is added to Table 1 for the sake of comparison. Namely, one can accept this result as a local conclusion.

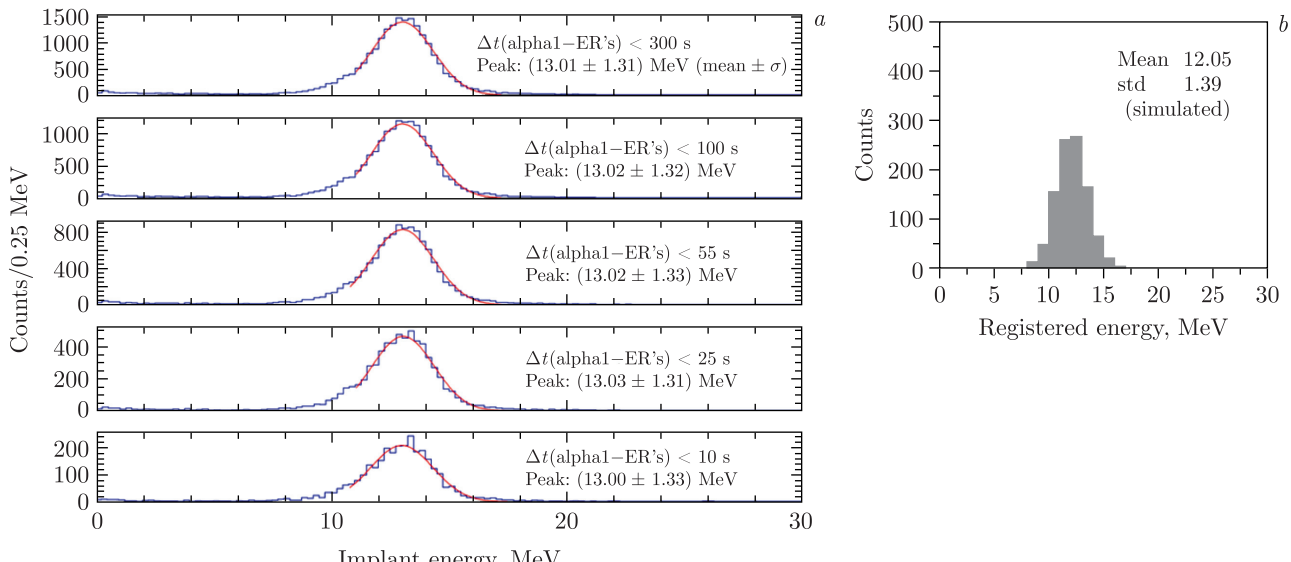

Fig. 5. *a*) Registered energy spectra for ^{254}No nuclei. Correlated times are: 300, 100, 55, 25 and 10 s, respectively (from top to bottom). *b*) Calculated spectrum of ^{254}No ER's using code from [21]

Table 2. **Parameters of recoiled superheavy nuclei (DSSD types of BB-17 and BB-24; see https://www.micronsemiconductor.co.uk). For all cases summary leakage current is lower than 45 μA**

Reaction	$E_{\rm calc}/std_{\rm calc}$	$d = E_{\rm reg} - E_{\rm calc}$	n (event)	Asymmetry $\frac{M_{\rm target}}{M_{\rm ion}}$	$d = \langle d_i \rangle$	$\sigma_{\rm center} = \frac{\sigma}{\sqrt{n}}$, according to CLT
^{238}U+^{40}Ar→Ds*	6.7/1.5	−0.4	2	5.95	⟨0.78⟩	1.06
^{242}Pu + ^{48}Ca → Fl*	11.8/1.6	+1.1	99	5.04		0.161
^{243}Am + ^{48}Ca → Mc*	12.4/1.5	+0.2	125	5.06		0.134
^{242}Pu + ^{50}Ti → Lv*	13.0/1.9	+1.8	5	4.84		0.850
^{238}U + ^{54}Cr → Lv*	18.5/2.0	+0.2	1	4.41		2.0
^{232}Th + ^{48}Ca → Ds*	13.1/1.2	+1.7	9	4.83		0.4
^{238}U + ^{48}Ca → Cn*	11.2/1.7	+0.9	16	4.96		0.425
^{208}Pb + ^{48}Ca → No* SHANS-2 setup, IMP, Lanzhou (2025)	12.1/1.39	+0.9	—	4.33	Not taken into account for d calculation	
^{242}Pu + ^{48}Ca → ^{287}Fl + 3n, DGFRS-1, PIPS detector, resistive layer, Canberra NV, Belgium	11.4/2.3	−0.4	25	4.84		0.46 $\langle\sigma_{\rm center}\rangle = 0.69$

1.2. Reaction ^{249}Bk $+^{50}$Ti $\to$ ^{296}119 $+ 3n$. Using the code for generating the spectrum of implanted heavy nuclei [21] and the data from Table 2, the recoiled nucleus spectrum of the isotope ^{296}119, produced in the fusion–evaporation reaction $^{249}\mathrm{Bk} + {}^{50}\mathrm{Ti} \to {}^{296}119 + 3n$, was generated. This reaction is considered a promising candidate for the synthesis of element $Z = 119$ at the DGFRS-2 setup in the near future, using an intense titanium ion beam at the DC-280 cyclotron. The resulting spectrum is shown in Fig. 6 along with a Gaussian fit. It is worth noting high value of the statistical criterion $R^2 = 0.992$.

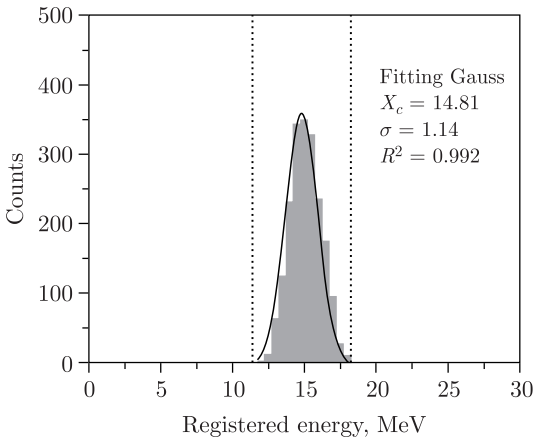

Fig. 6. Registered energy spectrum of implanted recoiled nuclei of the isotope ^{296}119 with the 99.7% confidence level interval indicated by dotted lines (reaction $^{249}\mathrm{Bk} + {}^{50}\mathrm{Ti} \to {}^{296}119 + 3n$)

Additionally, the 99.7% confidence interval is indicated by a dotted line, taking into account Table 2 (seventh row) and [36]. This value, along with its confidence intervals, can be useful for experimenters during the planned experiment at the DGFRS-2 setup in 2026–2027, as only a few decay events of the ^{296}119 nucleus are expected to be registered due to its very low production cross section [37–40]. This is especially relevant when applying the active correlations method, which is used to significantly suppress background products associated with the operation of the DC-280 cyclotron. Moreover, it is reasonable to adopt this interval as the first approximation for the search for ER–α correlated sequences in real time (the active correlations method). The second and subsequent approximations can be determined using a "flexible" algorithm that takes into account the "lost" time criterion [31–34, 41]. That is, the predicted total irradiation pause time for the target should not exceed a few percents, where this value is set in advance by the experimenter. In the mentioned works (tests), we selected the maximum number of irradiation stops as $N_{\max} = 4$ with a pause duration of 100 s. Thus, the maximum loss did not exceed 0.5% in those tests. It is important to note that the left boundary plays a crucial role, since the distribution of background signals shows a sharp decline toward higher registered energies. Naturally, the second iterative parameter, when applying the flexible algorithm in the active correlations

method, will be the value of the ER–α correlation interval. In addition, it should be kept in mind that expanding this calculation model for the spectrum of the $Z = 119$ nucleus in the reaction $^{249}\mathrm{Bk} + {}^{50}\mathrm{Ti} \rightarrow {}^{296}119 + 3n$, when approaching an irradiation dose by low-energy target-like products $D \rightarrow 10^8$ ions/cm^2, can be achieved by using the actual value of the surface recombination rate (see Sec. 3).

2. RADIATION EFFECTS

The primary manifestation of radiation damage to the detector during long-term experiments is the increase in leakage current. This parameter is commonly used to characterize the operational quality of the detector. For instance, these effects have been studied in [42, 43]. Notably, radiation damage ultimately limits the operational lifetime of silicon detectors in experiments involving ultraintense heavy-ion beams.

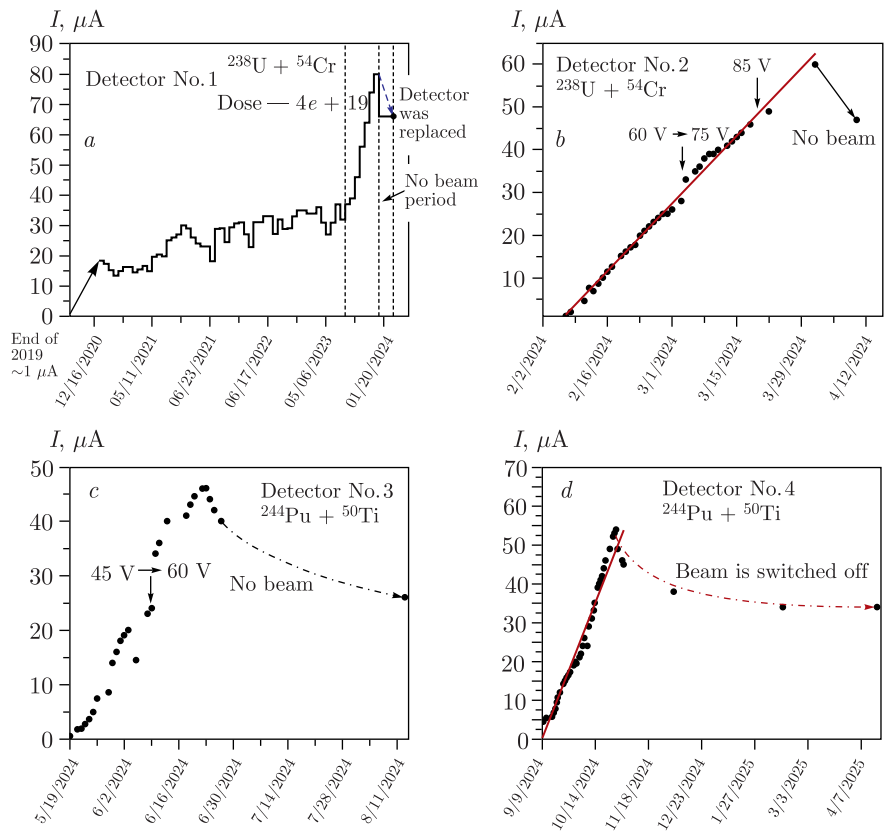

Fig. 7. Changes in leakage currents against date for detector No. 1 (*a*), detector No. 2 (*b*), detector No. 3 (*c*), and detector No. 4 (*d*)

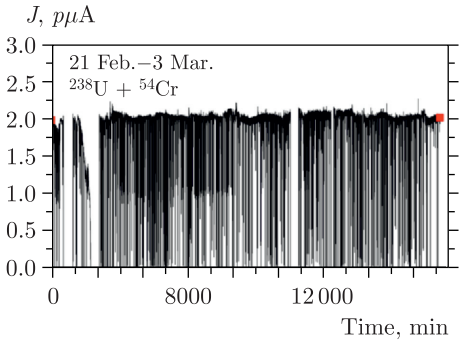

Fig. 8. Typical value of projectile beam intensity against time in $^{238}U + ^{54}Cr \to Lv^*$ experiment (2023)

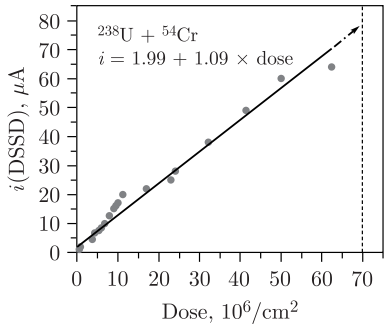

Fig. 9. Dependence of leakage current on effective dose value

Figure 7 illustrates the performance of DSSD detectors Nos. 1–4 in experiments conducted using the DGFRS-2 setup [44] over the past four years. The abscissa represents measurement dates, while the typical "live" beam time (2–3 $p\mu$A) spanned 2–4 months per year. Target-like particles with energies between 0.5–5 MeV (comprising ~ 95–98% of the detector load) were the primary contributors to the detector's workload. Figure 7, *b* displays the relationship between leakage current and dose for detector No. 2. The estimated dose accuracy was within $\sim 20\%$. In Fig. 7, an increase in detector leakage current can be observed as the experiment progresses. It increases by approximately 1 μA per day at a temperature of $\sim 27\,^{\circ}$C. The dependence of leakage current on dose can be seen in Fig. 9.

As for Fig. 8, it demonstrates the long-term stability of the beam, which in turn facilitates the near-future development of an analytical model for the generation/relaxation of recombination centers.

Of course, one can easily see that the degradation process of the DSSD detector is quite different for experiments with ^{48}Ca compared to those with ^{50}Ti and ^{54}Cr projectiles. (Dose $\sim 7e + 7$ corresponds to the limit for peak stability region.)

From the perspective of the practical application of silicon detectors in experiments with ultraintense heavy ion beams — specifically for predicting the detector's *in situ* lifetime — the dependences (systematics) presented in Fig. 9 are of key importance. This figure illustrates the rate at which the dose approaches the "critical" value, as discussed in [43, 45].

3. RESULTS AND DISCUSSION IN BRIEF

All measured amplitudes of recoiled nuclei were obtained strictly in the range of up to an effective dose of $7 \cdot 10^7$ ions/cm^2. Note that percentage points of events are outside the registered by the DSSD interval of energy values calculated using the code reported in [21, 38]. Table 2 presents typical

deviations of the average value of the distribution amplitudes from the value calculated for reactions listed in the table. The weighted average of the adjustment was

$$\Delta E = \frac{\sum N_i \, \Delta_i}{\sum N_i} = 0.67,$$

which will be used in subsequent experiments, namely, in the form of a correction formula

$$\Delta_{\text{corr}} = 0.28 \times E_{\text{in}} - 0.006 \times E_{\text{in}}^2 - 0.3.$$

Here E_{in} is the energy of the recoiled nucleus at the input of the DSSD detector in MeV, and the average value of the deviation is calculated by the formula

$$D = \frac{\sum d_i \, h_i}{\sum h_i},$$

whereas the statistical weight of the deviation is taken as $h_i = \dfrac{\sqrt{N}}{\sigma_i}$ [14].

It should be noted that the issue of radiation damage scenarios in silicon detectors under exposure to light particles — hadrons — has been studied for the past 20 years within the RD50 collaboration at CERN [46, 47]. The impact of heavier particles, such as ions of various elements, became relevant only a few years ago in connection with the design of the international accelerator complex FAIR (GSI, Darmstadt, Germany) [48, 49]. It is important to emphasize that in our case we deal with extremely hard radiation (e.g., ^{238}U at ~ 6 MeV has a penetration depth of about one micron, meaning that defect formation occurs in the near-surface region). Even if a single implanted uranium atom creates just one level in the silicon bandgap, then at a dose of about $7 \cdot 10^7$ cm^{-3}, the concentration of levels will be $7 \cdot 10^{11}$ cm^{-3}. For comparison, the donor concentration in n-type silicon with a resistivity of approximately 8 k$\Omega\cdot$ cm is equal to $\sim 2.8 \cdot 10^{11}$ cm^{-3}. The dynamics of the transformation of the n-type semiconductor are described in [50]. Typically, the degradation scenario includes information on how detector characteristics (generation current, electric field, and several others) change with increasing radiation dose. The role of near-surface defects under the impact of heavy ions is discussed in [51].

It was Kurokawa [36] who first recognized the importance of the non-ionizing energy loss value (Δ_{st}) along the ion path in silicon as a critical parameter. In [37], critical dose values are presented for three groups of ionizing particles: protons, α particles, and fission fragments. In Fig. 10, a second-order polynomial extrapolation is shown to predict the critical dose for 6-MeV ^{238}U ions using both the Wilkins [52] and the Ogihara formula [53]. The formula is as follows:

$$\Delta_{\text{st}} = 2.33 \cdot 10^{-4} \, A^{0.7} Z^{1.2} E^{0.5},$$

where A is mass number, E is energy in MeV, and Z is atomic number.

Therefore, as a local summary, one can state that the critical dose for 6-MeV uranium ions is less than 10^8/cm^2. The same result can be ob-

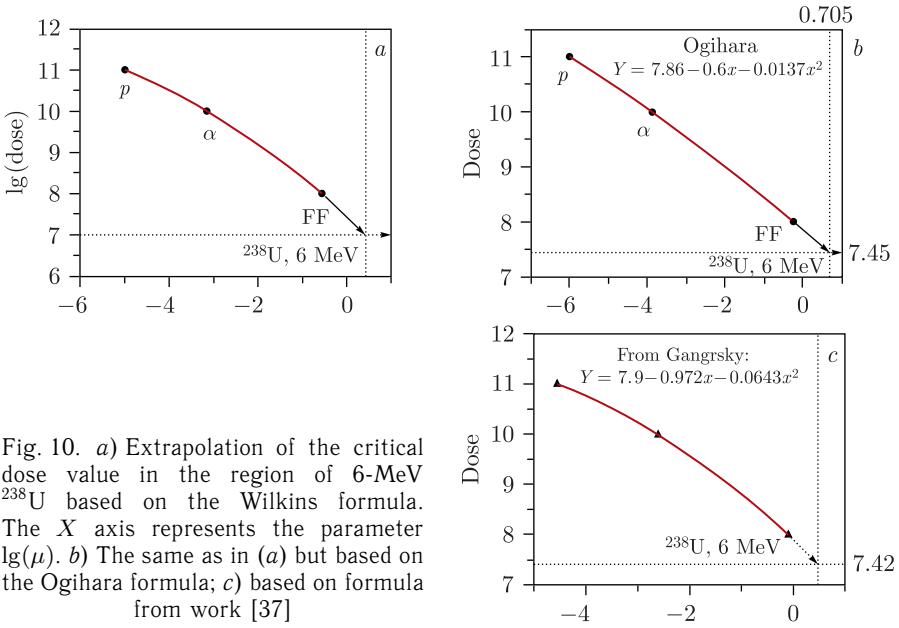

Fig. 10. *a*) Extrapolation of the critical dose value in the region of 6-MeV ^{238}U based on the Wilkins formula. The X axis represents the parameter $\lg(\mu)$. *b*) The same as in (*a*) but based on the Ogihara formula; *c*) based on formula from work [37]

tained using the electric field-independent formula for the pulse height defect from [37, 54], which is

$$w = \left[\frac{6w}{w+8} + \frac{B}{1+525w^{-1.407}}\right] \Big/ K,$$

$$w = K\,E;$$

$$K = 6.53\frac{10^4}{\left[Z(Z^{2/3}+5.81)^{1/2}(A+28.1)\right]},$$

where $B = 18$ [55].

Our experience shows that for our DSSD back strips the typical change in FWHM ranges from 33–35 to 55–65 keV. While this is not critical, the peak positions are considered to be unstable.

Note, additionally, that one can obtain nearly the same result by using TRIM calculations [56] of the average number of primary vacancies as the X axis for interpolation, as shown in Fig. 11. A Monte Carlo calculation using event-by-event files from the experiment can be performed (the first 2000 events were taken from the working file PuTi.558 of the ^{242}Pu + ^{50}Ti → → Lv* reaction). Specifically, each event can be used to calculate both the incoming energy and the individual number of primary vacancies to estimate the effective mean number of vacancies. Of course, each registered energy amplitude should also be corrected individually for the pulse-height effect. For the dependence of the number of vacancies on the registered incoming energy, it is reasonable to apply an analytical approximation.

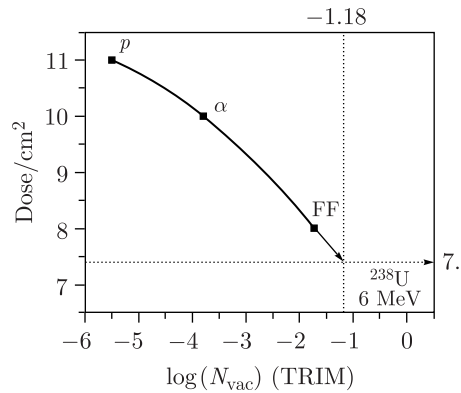

Fig. 11. Dose per cm^2 against primary average vacancies number as a parameter (X axis) for extrapolation procedure

The use of primary defects, as calculated by TRIM (Fig. 11), allows for an extrapolation that is independent of the NIEL (Non-Ionizing Energy Loss) method. Naturally, not all primary defects create recombination centers within the silicon forbidden gap. However, as a first-order approximation, it is reasonable to assume that the fraction of defects forming effective recombination levels is proportional to the number of primary defects. Therefore, the number of primary defects can be used as a basis for systematics (X axis).

The fact that the obtained dose value of approximately $\sim 7 \cdot 10^7$ cm^{-2} coincides with the result derived using the NIEL method makes this approach self-consistent.

As for radiation restrictions on the use of this type of detectors, it is obvious that for more symmetrical ion/target combinations the number of cases of achieving doses of $\sim 10^8$ ions/cm^2 this time is significantly shorter. Obviously, when working with heavy-ion beam intensities of $\sim 10\, p\mu$A and more, a number of radical changes in the detection system and the DGFRS-2 separator itself will be strictly necessary. These changes are not considered in this article, but we note the unacceptability of trivial approaches, for example, the use of additional absorbers. The reason is a notable decrease in the nuclide implantation depth, which reduces significantly the efficiency of recording the coordinate of a composite signal of α decay (focal DSSD + Side detector, see Fig. 1).

During the defect formation process, generation–recombination levels are created within the silicon bandgap, which leads to an increased significance of generation–recombination processes, including an increase in leakage current.

For the reverse current arising due to generation–recombination processes in the depletion region, one can write:

$$J_{g-r} = \frac{en_i d}{\tau_{\text{eff}}},$$

where e is the elementary charge, d is the width of the depletion layer, n_i is the intrinsic carrier concentration, and τ_{eff} is the effective lifetime of electron-hole pairs [57–59].

It is evident that after the beam is turned off not only the number of recombination levels increases — leading to a decrease in the effective carrier lifetime and, consequently, an increase in leakage current — but also some of the newly formed levels within the silicon bandgap undergo relaxation, as observed in the figures above.

It is important to note, however, that this standard approach does not explain the observed saturation in the decrease of leakage current after the end of the experiment.

Here, one must take into account that a uranium ion dose of approximately $\sim 10^8$ cm^{-2} (or of plutonium or californium) at an energy of about 6 MeV and a range of approximately one micron results in the formation of a non-relaxing level of defects (surface states). This leads to a significant increase in surface recombination velocity and, consequently, not only to an increase in leakage current but also to additional charge loss in alpha decays, with a relative magnitude of [60, 61]

$$\Delta\lambda = \frac{\Delta S\, t_P}{R}.$$

Here $\Delta S = S_{\text{finish}} - S_{\text{initial}}$ is a difference in the final and initial value of surface recombination parameter, R is range of alpha particle, and t_P is plasma time according to [62].

For a $p{-}n$ junction made with planar technology, typical values of lambda and plasma time are approximately 0.2% and 6 ns, respectively [63], that is,

$$S_{\text{initial}} = \frac{0.002 \cdot 25 \cdot 10^{-4}\ \text{cm}}{7 \cdot 10^{-9}\ \text{s}} \approx 800\ \text{cm/s}.$$

When, for example, we observe about ~ 100 keV displacement in 6.06-MeV alpha peak, we really have

$$S_{\text{finish}} \approx 800 + \frac{100 \cdot 25 \cdot 10^{-4}}{6060 \cdot 6 \cdot 10^{-9}} \approx 10^4\ \text{cm/s}.$$

As a preliminary conclusion of this section, the following points should be mentioned:

— The system has demonstrated good performance and will continue to be used in its current form for asymmetric reactions (e.g., ^{48}Ca, see Fig. 5, *a*) in long-term SHE synthesis experiments;

— For reactions involving ^{50}Ti and ^{54}Cr ions, reasonable but not radical adaptation scenarios are possible, as outlined in Table 3;

— As long as the mitigation strategies described in Table 3 remain effective, we do not foresee any radical changes in the near future (up to $\sim$ 2026).

And, of course, in any case, a compromise should be reached between the chosen action (1–5) and achieving the maximum possible implantation depth.

Table 3. **Reasonable scenarios to improve the detection system**

Action	Advantage	Disadvantage	An assumed period
1) To set degrader (mylar, aluminum foil)	The simplest	It decreases implantation depth → therefore, to decrease part of energy signal in DSSD when detecting escaping decay	In stage of discussion
2) To change pentane pressure up to 1.5–2.2 Torr	Simple and in contrast to (1) is more flexible	The same as (1)	Late 2025 or early 2026
3) To optimize collimators behind rotating target and some other magnet optics	No need of beam time (to a first approximation). See, e.g., [64]	Beam time test is strongly required after finishing development process	Early 2026
4) To increase a little bit (up to 0.8–1 Torr) H_2 pressure in the DGFRS-2	Highly likely the same as (2). Can be considered as complementary to (2)		Late 2025 or early 2026
5) "Soft" annealing, 50–80 °C	Typical procedure	No quarantee of non-destruction of contacts	No plans

4. SUMMARY

In long-term experiments conducted using the DGFRS-2 setup, spectra of recoiled superheavy nuclei with $Z = 114-116$ were measured in [17–20] and found to be in good agreement with computer simulations, with discrepancies limited to a small empirical correction of approximately 6%. Regarding the negative radiation-induced changes in the leakage current of DSSD detectors, at heavy-ion intensities on the order of 2–3 $p\mu$A (using ^{54}Cr and ^{50}Ti projectiles), the leakage current can increase by approximately 1 μA per day at a temperature of $\sim 27\,^{\circ}$C. An attempt was made to roughly estimate the radiation dose limit for DSSD detector applications during irradiation with low-energy target-like products.

The detection system can be improved without radical changes for long-term experiments with Ti and Cr ions at intensities above 2–3 $p\mu$A.

Furthermore, we will continue to enhance the method for calculating spectra of implanted recoil nuclei in silicon detectors, including the use of more asymmetric distributions for fluctuations in non-ionizing energy loss and taking into account other phenomena that lead to approximately 2.8% of events deviating from the main dependence.

Acknowledgements. This work was supported by the Russian Science Foundation and National Natural Science Foundation of China (grant No. 25-42-00003).

We thank Dr. A. Sokhatsky for assistance with radiation defects, Dr. V. Salamatin for assistance in upgrading the code simulating the spectrum of heavy nuclei, and Dr. Z. Y. Zhang (IMP, China) for the presented spectra of ^{254}No from the SHANS-2 experiment.

APPENDIX 1
ON THE EFFECTIVE ENERGY VALUE OF THE TARGET-LIKE BACKGROUND IONS

The primary background load in experiments using gas-filled separators consists of target-like ions with low energies. For example, in the reaction $^{238}\mathrm{U} + ^{54}\mathrm{Cr} \to \mathrm{Lv}^*$, the fraction of events in the energy range from approximately 500 keV to 5 MeV accounts for about 95% of the total number of pulses. Accordingly, the effective average registered energy of target-like ions is roughly ~ 2.3 MeV.

Using an iterative procedure (Fig. 12) described below and applying the Wilkins formula [54], we estimate the effective average incoming energy to be approximately ~ 6 MeV. This value is used above for a rough estimation of the radiation damage process.

Here, E^i_{reg} is the energy value at the i-th iteration number, $E^{\mathrm{meas}}_{\mathrm{reg}}$ is the measured average value, and ε is a predefined small positive value.

APPENDIX 2
A FEW WORDS ADDITIONALLY ABOUT RADIATION DAMAGES IN n-SILICON

It is generally accepted (see, for example, [49, 50]) that defect formation leads to two key processes affecting the effective charge concentration N_{eff}, which in turn alters all electrophysical characteristics of the detector: donor removal and acceptor introduction. These processes are described within the framework of the Hamburg model, according to which the change in effective concentration with increasing radiation dose is given by the

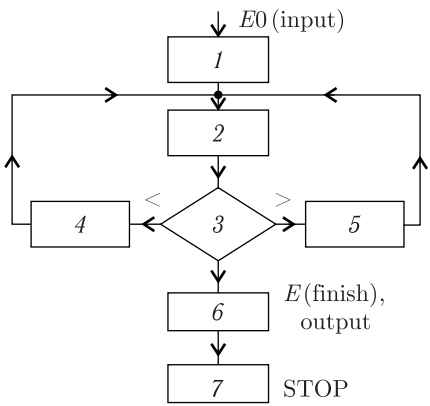

Fig. 12. Flowchart of the iteration process. *1* — input of ion energy — zero approximation, *2* — calculation of energy loss value using Wilkins formula, *3* — comparison of registered energy value with measured one, *4* — case "*greater*" ($E^i_{\mathrm{reg}} > E^{\mathrm{meas}}_{\mathrm{reg}}$), *5* — case "*lower*" ($E^i_{\mathrm{reg}} < E^{\mathrm{meas}}_{\mathrm{reg}}$), *6* — case "*ok*" ($|E^i_{\mathrm{reg}} - E^{\mathrm{meas}}_{\mathrm{reg}}| < \varepsilon$), output energy value, *7* — stop

formula $N_{\text{eff}} = N_0 e^{-\text{CF}} - \beta F$. Here, N_0 is the effective concentration of the unirradiated structure ($N_0 = N_d$), C is a coefficient characterizing donor removal, and β is a coefficient characterizing acceptor introduction. It is important to note that at a certain irradiation dose (FSCSI) the effective concentration becomes negative. This phenomenon is known as *space charge sign inversion* (SCSI) and reflects compensation in the irradiated material.

Returning to our case: of course, the SCSI point is unlikely to be reached in our experiment, or even approached. In the context of precision spectroscopy, the need to replace the detector arises much earlier. However, based on the above, we can propose the following mnemonic (schematic) for the defect formation process.

Figure 13 illustrates the transformation of the irradiated detector (more precisely, the near-surface region): *1* → *2* → *3*.

Naturally, starting from region *2*, the value of the recombination constant increases, and we do not exclude the possibility of a sharp rise during the transition from region *2* to *3*. Furthermore, the substitution of donors in the near-surface region leads to the formation of a dead layer, which becomes significantly thicker than its initial value.

Of course, in that context, we also plan to extend the application range (up to $1 \cdot 10^8$ ++ ions) of our code for generating the energy spectrum of measured recoiled heavy nuclei implanted into a silicon detector. This will naturally require a more sophisticated approach to modeling the pulse height defect in Si detectors.

Additionally, it is important to note that the Hamburg model equation is written in an integral form. However, we believe that in our case any defect formation model should fundamentally be differential in nature and account for relaxation processes (clearly visible in Fig. 5, *c*, *d*).

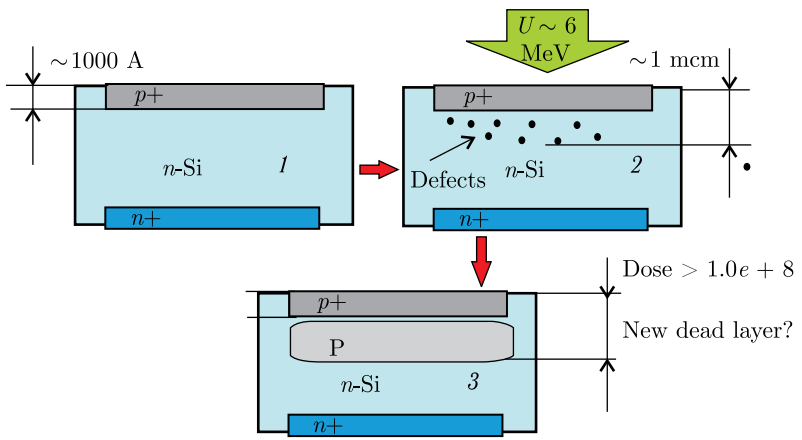

Fig. 13 (color online). Schematics of p–n junction degradation process

And, of course, one intermediate state is quite reasonable between $|2\rangle$ and $|3\rangle$, which is in fact formatted as multi $|p\rangle$-islands structure.

APPENDIX 3
THE "ExTekh" ICS-119 MODULE FOR TESTING REAL-TIME ER–α CORRELATION SEARCH ROUTINES

The 1M CAMAC ICS-119, produced by "ExTekh" [65], is used in 2025 to generate correlated sequences that imitate SHE α decay. Its two output DB-37 connectors are linked to the ADP-16 input connector [65] via a 0.5–1 m cable. By pressing the front panel button or, alternatively, by processing the NA(0)F(25) function, a single α-decay sequence is generated for the selected ADP. The shape of the ICS-119 signal approximately corresponds to that of a charge-sensitive preamplifier, with a decay time of about 100 μs. Note that for the DGFRS-2 spectrometer, the front strip signal has positive polarity, whereas the back strip signal has negative polarity.

The pre-set parameters for the decay chains are configured as follows:

— NA(0)F(10): Resets all parameters.

— NA(0)F(10): Writes a value to the coordinate register (X and Y), using four bits for each direction.

— NA(1)F(16): Writes the first time interval (t_1) with a step size of 0.1 μs.

— NA(2)F(16): Writes the second time interval (t_2) with a step size of 0.01 ms.

— NA(3)F(16): Writes the amplitude value (range 0–2047).

Functions to read the pre-set parameters are also available. A 100-Hz signal can be observed on the LEMO output of the rear panel. Its amplitude corresponds to the value set by the NA(3)F(16) function described above. If the C++ program [21] for the DGFRS-2 analog spectrometer detects a correlated sequence, it changes the state of the "ExTekh-1M" BTP (beam terminator actuator) output from +3.5 to 0 V.

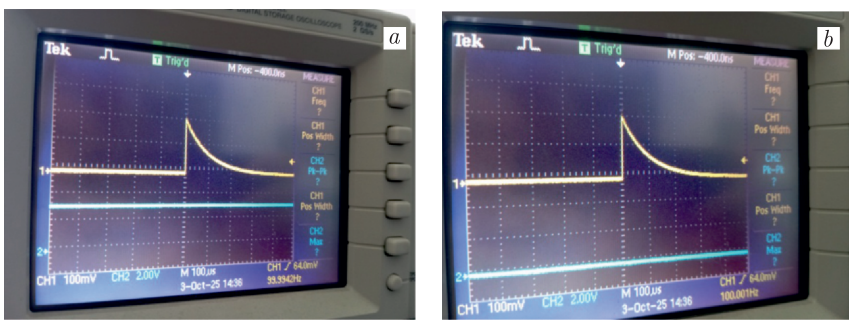

Fig. 14 (color online). Yellow line — preamplifier like signal from ICS-119, blue lines correspond to "beam on" (*a*) and "beam off" (*b*) phases, respectively

APPENDIX 4

When preparing this manuscript, long-term experiment $^{237}Np + ^{48}Ca$ has been performed. DSSD detector No. 4 (see Table 3 and Fig. 7, *d*) was successfully used as a focal plane detector in that experiment. An additional degrader of 0.8-μm Al foil was placed in front of detecting module. The initial value of leakage current was ~ 26 μA. The change rate for that value is presented in the Table 4 for ~ 3 $p\mu$A $^{48}Ca^{+10}$ beam intensity.

Table 4. **The leakage current of the detector No. 4**

Date	10.09.25	17.09	20.09	17.10	24.10	26.10	28.10	29.10
Leakage current I, μA (70 V)	26.2	32.3	35	37.3	41.2	42.1	43.2	43.2

REFERENCES

1. *Oganessian Yu. Ts., Rykaczewski K. P.* A Beachhead on the Island of Stability // Phys. Today. 2015. V. 68, Iss. 8. P. 32–38; https://doi.org/10.1063/PT.3.2880.
2. *Oganessian Yu. Ts., Utyonkov V. K.* Superheavy Element Research // Rep. Prog. Phys. 2015. V. 78. P. 036301; doi: 10.1088/0034-4885/78/3/036301.
3. *Oganessian Yu. Ts., Utyonkov V. K.* Superheavy Nuclei from ^{48}Ca-Induced Reactions // Nucl. Phys. A. 2015. V. 944. P. 62; https://doi.org/10.1016/j.nuclphysa.2015.07.003.
4. *Eichler R., Brühle W., Dressler R., Duelmann Ch. E. et al.* Chemical Characterization of Bohrium (Element 107) // Nature Lett. 2000. V. 407. P. 63–65.
5. *Oganessian Yu. Ts. et. al.* Synthesis of the Isotopes of Elements 118 and 116 in the ^{249}Cf and $^{245}Cm + ^{48}Ca$ Fusion Reactions // Phys. Rev. C. 2006. V. 74, No. 4. P. 044602.
6. *Oganessian Yu. Ts. et. al.* Experiments on the Synthesis of Element 115 in the Reaction $^{243}Am(^{48}Ca, xn)^{291-x}115$ // Phys. Rev. C. 2004. V. 69. P. 021601.
7. *Oganessian Yu. Ts. et al.* Synthesis of Elements 115 and 113 in the Reaction $^{243}Am + ^{48}Ca$ // Phys. Rev. C. 2005. V. 72. P. 034611.
8. *Oganessian Yu. Ts. et al.* Synthesis of a New Element with Atomic Number $Z = 117$ // Phys. Rev. Lett. 2010. V. 104. P. 142502.
9. *Stavsetra L. et al.* Independent Verification of Element 114 Production in the $^{48}Ca + ^{242}Pu$ Reaction // Phys. Rev. Lett. 2009. V. 103. P. 132502.
10. *Khuyagbaatar J. et al.* $^{48}Ca + ^{249}Bk$ Fusion Reaction Leading to Element $Z = 117$: Long-Lived α-Decaying ^{270}Db and Discovery of ^{266}Lr // Phys. Rev. Lett. 2014. V. 112. P. 172501.
11. *Kosuke Morita et al.* Experiment on the Synthesis of Element 113 in the Reaction $^{209}Bi(^{70}Zn, n)^{278}113$ // J. Phys. Soc. Jpn. 2004. V. 73, No. 10. P. 2593–2596.
12. *Gates J. M. et al.* Decay Spectroscopy of Element 115 Daughters: $^{280}Rg \rightarrow ^{276}Mt$ and $^{276}Mt \rightarrow ^{272}Bh$ // Phys. Rev. C. 2015. V. 92. P. 021301.
13. *Luo D. W. et al.* The Implementation of a Focal Plane Detector System at the Gas-Filled Recoil Separator for the Decay Studies of Heavy Nuclei // Nucl. Instr. Meth. A. 2025. V. 1075. P. 170333; https://doi.org/10.1016/ j.nima.2025.170333.

14. *Zhishuai Ge, Gen Chang, Shihui Cheng, Tsyganov Yu. S., Feng-Shou Zhang.* Calculation of the α-Decay Properties of $Z = 120, 122, 124, 126$ Isotopes // Chin. Phys. C. 2020. V. 44, No. 10. P. 1–17; doi: 10.1088/1674-1137/44/10/ 10410.
15. *Zhishuai Ge et al.* Effect of Shell Corrections on the α-Decay Properties of $^{280-305}$Fl Isotopes // Phys. Rev. C. 2018. V. 98. P. 034312.
16. *Gulbekian G. G., Dmitriev S. N., Oganessian Yu. Ts. et al.* // Proc. of the 21st Intern. Conf. on Cyclotrons and Their Applications. 2016. P. 278–280.
17. *Oganessian Yu. Ts. et al.* First Experiment at the Superheavy Element Factory: High Cross Section of ^{288}Mc in the ^{243}Am $+^{48}$Ca Reaction and Identification of the New Isotope ^{264}Lr // Phys. Rev. C. 2022. V. 106. L031301; https://doi.org/10.1103/ PhysRevC.106.L031301.
18. *Oganessian Yu. Ts. et al.* Investigation of ^{48}Ca-Induced Reactions with ^{242}Pu and ^{238}U Targets at the JINR Superheavy Element Factory // Phys. Rev. C. 2022. V. 106. 024612.
19. *Oganessian Yu. Ts. et al.* New Isotope ^{286}Mc Produced in the ^{243}Am $+^{48}$Ca Reaction // Phys. Rev. C. 2022. V. 106. 064306; https://doi.org/10.1103/PhysRevC.106.064306.
20. *Oganessian Yu. Ts. et al.* New Isotope ^{276}Ds and Its Decay Products ^{272}Hs and ^{268}Sg from the ^{232}Th $+^{48}$Ca Reaction // Phys. Rev. C. 2023. V. 108. 024611.
21. *Ibadullayev D. et al.* Specific Moments in Detection of Superheavy Nuclei: DGFRS-2 Spectrometer // JINST. 2023. V. 18. P05010; doi: 10.1088/1748-0221/18/05/P05010.
22. *Ibadullayev D. et al.* Flexible Algorithms for Background Suppression in Heavy Ion Induced Nuclear Reactions // Eurasian J. Phys. Funct. Mater. 2022. V. 6. P. 18–31.
23. *Ibadullayev D. et al.* $E-\Delta E$ Detection Module of DGFRS-2 Setup // Appl. Rad. Isot. 2024. V. 212. P. 111431; https://doi.org/10.1016/j.apradiso.2024.111431.
24. *Shinichiro Takeda et al.* Development of Double-Sided Silicon Strip Detectors (DSSD) for a Compton Telescope. SLAC-PUB-12927. 2007.
25. *Gross C. J. et al.* Performance of the Recoil Mass Spectrometer and Its Detector Systems at the Holifield Radioactive Ion Beam Facility // Nucl. Instr. Meth. A. 2000. V. 450. P. 12–29.
26. *Grzywacz R. et al.* Rare Isotope Discoveries with Digital Electronics // Nucl. Instr. Meth. B. 2007. V. 261. P. 1103–1106.
27. *Gregor E. T.* The Double-Side Silicon Strip Detector with Excellent Position, Energy and Time Resolution. Bachelor Thesis, 2009.
28. *Gorshkov A. V.* A New Focal Plane Detector for the Gas-Filled Separator TASCA. Doctoral Thesis. TU Munich, 2010.
29. *Yakushev A. B.* Private Commun. 2009.
30. *Tsyganov Yu. S. et al.* Review of Some Specific Features on the Detecting of Heavy Ions; ArXiV2305.13344.
31. *Tsyganov Yu. S. et al.* Development of the Active Correlations Method: Theoretical and Methodical Aspect // Phys. Part. Nucl. 2018. V. 49, No. 6. P. 1624–1642.
32. *Tsyganov Yu. S., Ibadullayev D. et al.* New Analog Spectrometer of the DGFRS-2 Setup for Real-Time Searching of ER–α and α–α Correlated Sequences in Heavy-Ion Induced Complete Fusion Nuclear Reactions // Acta Phys. Polon. B. Proc. Suppl. 2021. V. 14, No. 4. P. 767–774.

33. *Tsyganov Yu. S. et al.* DSSD Based Detection System of the DGFRS-2 Setup: Design, Results, Developments // Phys. At. Nucl. 2025. V. 88, No. 2. P. 1–7.
34. *Ibadullayev D. et al.* YDA C++ Program Package for Operating with a New Analog Spectrometer of DGFRS-II Setup // Acta Phys. Polon. B. Proc. Suppl. 2021. V. 14. P. 873–878.
35. *Alexandrov A. A.* Developments of Semiconductor Spectrometry of Heavy Ions. PhD Thesis. MEPhI, Moscow, 1989 (in Russian).
36. *Hudson D. J.* Lectures on Elementary Statistics and Probability. Geneva: CLT, 1967.
37. *Oganessian Yu. Ts. et al.* Investigation of Reactions with ^{50}Ti and ^{54}Cr for the Synthesis of New Elements // Phys. Rev. C. 2025. V. 112. P. 014603.
38. *Utyonkov V. K.* Private Commun. 2020.
39. *Ibadullayev D.* // Report on Topical Workshop on Superheavy Element Synthesis, July 7–10, 2024, Beijing Normal University, Beijing, China.
40. *Kovrizhnykh N.* // Rep. TASCA Workshop, April 23, 2025, GSI, Darmstadt, Germany.
41. *Ibadullayev D. et al.* Flexible Scenario for Background Suppression in Heavy Element Research // Phys. At. Nucl. 2022. V. 85, No. 12. P. 1981–1987.
42. *Kurokawa M. et al.* Radiation Damage Factor for Ion-Implanted Silicon Detectors Irradiated with Heavy Ions // IEEE Trans. Nucl. Sci. 1995. V. 42, No. 3. P.163–166.
43. *Gangrsky Yu. P. et al.* Registration and Spectrometry of Fission Fragments. M.: Energoizdat, 1992. 312 p. (in Russian).
44. *Oganessian Yu. Ts. et al.* DGFRS-2 — A Gas-Filled Recoil Separator for the Dubna Superheavy Element Factory // Nucl. Instr. Meth. A. 2022. V. 1033. P. 166640; https://doi.org/10.1016/ j.nima.2022.166640.
45. *Kushniruk V. F.* On Charge Losses in Semiconductor Detectors during the Detection of Highly Ionizing Particles. JINR Commun. P13-11933. Dubna, 1978.
46. *Van Lint V. A.* The Physics of Radiation Damage in Particle Detectors // Nucl. Instr. Meth. A. 1987. V. 253. P. 453–459; https://doi.org/10.1016/0168-9002(87)90532-8.
47. *Lindström G. et al.* Radiation Hard Silicon Detectors — Development by the RD48(ROSE) Collaboration // Nucl. Instr. Meth. A. 2001. V. 466, Iss. 2. P. 308–326.
48. https://fair-center.eu/en/public/what-is-fair.html.
49. *Eremin V. et al.* Beam Tests of Full Size Prototypes Detectors for TOF Heavy-Ions Diagnostics in Super-FRS // JINST. 2017. V. 12. P. C03001.
50. *Mol M.* Radiation Damage in Silicon Particle Detector-Microscopic Defects and Macroscopic Properties. PhD Thesis. Hamburg, 1999. 251 p.
51. *Bugrov V. N., Karamyan S. A.* Destructive Action of Heavy Ions to Monocristals. JINR Preprint P14-84-731. Dubna, 1984.
52. *Wilkins B. D. et al.* Pulse-Height Defects for Heavy Ions in a Silicon Surface-Barrier Detector // Nucl. Instr. Meth. 1971. V. 92. P. 381.
53. *Ogihara M., Nagashima Y., Galster W., Mikumo T.* Systematic Measurements of Pulse Height Defects for Heavy Ions in Surface-Barrier Detectors // Nucl. Instr. Meth. Phys. Res. A. 1986. V. 251, No. 2. P. 313–320.
54. *Kaufman S. B. et al.* A Calibration Procedure for the Response of Silicon Surface-Barrier Detectors to Heavy Ions // Nucl. Instr. Meth. 1974. V. 115. P. 47–55.

55. *Shmitt R. P. et al.* Nuclear Relaxation Phenomena, Diffusion and Orbiting in the Reaction ^{107,109}Ag+^{84,86}Kr at 7.2 MeV/nucleon // Nucl. Phys. A. 1977. V. 279. P. 141–158.
56. *Ziegler J. F.* Code SRIM-2013; http://www.srim.org.
57. *Gnuchev N. M.* Electronic Devices: Physical Foundations of Electronics / Ed. by Politechnical University, Saint Petersburg, 2013. P. 1–94 (in Russian).
58. *Pikus G. E.* Fundamentals of Semiconductor Detector Theory. M.: Nauka, 1965. P. 1–443.
59. *Lynch P., Nicolaides A.* Worked Examples in Physical Electronics. London: Harrap, 1972. P. 1–259.
60. *Kushniruk V. F., Kharitonov Yu. P., Tsyganov Yu. S.* A New Approach to the Recombination Component of Pulse Height Defect. JINR Commun. E7-91-75. Dubna, 1991. P. 195–196.
61. *Kushniruk V. F., Tsyganov Yu. S.* Recombination Charge Losses in Silicon Detectors of Heavy Ions // Instr. Exp. Tech. 1998. V. 41, No. 3. P. 320–322.
62. *Seibt W., Sundström K. E., Tove P. A.* Charge Collection in Silicon Detectors for Strongly Ionizing Particles // Nucl. Instr. Meth. 1973. V. 113. P. 317–324.
63. *Tsyganov Yu. S.* JINR Commun. P13-96-430. Dubna, 1996.
64. *Solovyev D. I., Kovrizhnykh N. D.* Simulations of Recoil Trajectories in Dubna Gas-Filled Recoil Separator 2 by GEANT4 Toolkit // J. Instrum. 2022. V. 17. P07033.
65. ICS-119, BTP "ExTekh-1M" Manuals, Dubna, 2025. P. 1–5.

Received on September 24, 2025.

Редактор *Е. И. Крупко*

Подписано в печать 24.11.2025.
Формат 60 × 90/16. Бумага офсетная. Печать цифровая.
Усл. печ. л. 1,75. Уч.-изд. л. 1,90. Тираж 100 экз. Заказ № 61221.

Издательский отдел Объединенного института ядерных исследований
141980, г. Дубна, Московская обл., ул. Жолио-Кюри, 6.
E-mail: publish@jinr.ru
www.jinr.ru/publish/